Geology, Geophysics & Environment 2026, vol. 52 (2): 109–129

Petrophysical and geomechanical characterization of coal-bearing strata in the Upper Silesian Coal Basin based on well logs and core data

Anita Lis-Śledziona[1], Weronika Kaczmarczyk-Kuszpit[2], Małgorzata Słota-Valim[3]

[1] *Instytut Nafty i Gazu – Państwowy Instytut Badawczy, Pion Poszukiwań Złóż Węglowodorów, Krakow, Poland, e-mail: lis-sledziona@inig.pl, ORCID ID: 0000-0003-3067-3014*
[2] *Instytut Nafty i Gazu – Państwowy Instytut Badawczy, Pion Poszukiwań Złóż Węglowodorów, Krakow, Poland, e-mail: kaczmarczyk-kuszpit@inig.pl, ORCID ID: 0000-0002-7458-1966*
[3] *Instytut Nafty i Gazu – Państwowy Instytut Badawczy, Pion Poszukiwań Złóż Węglowodorów, Krakow, Poland, e-mail: slota-valim@inig.pl, ORCID ID: 0000-0002-5915-7614*

Received: 22 January 2026; accepted: 7 April 2026; first published online: 28 May 2026

Abstract: Reducing methane emissions from hard coal mining and optimizing its utilization are currently key objectives in the Polish energy transition. This study aims to support these efforts by identifying methane accumulation zones and potential migration pathways and assessing the stability of the rock mass. We present an integrated petrophysical and geomechanical analysis based on geophysical wireline logs calibrated with laboratory measurements from six deep surface and underground boreholes in the Upper Silesian Coal Basin (USCB), one of Europe's most important coal-bearing regions. The analysis includes the estimation of porosity, permeability, bulk density, Young's modulus, Poisson's ratio, and compressive and tensile strength, with attention to lithological heterogeneity. Rock types were classified using cross-plotting and statistical tagging techniques, enabling the definition of five major rock types: coal, shale-coal, sandstone, shaly sandstones, and mudstone. Permeability was calculated from porosity using empirical formulas calibrated with core data. Elastic parameters were derived from acoustic and density logs, then corrected to static values using laboratory data. The results reveal that coal rock exhibits the highest permeability, despite having moderate porosity, while sandstones show low permeability due to compaction and cementation. This well log-scale parametric model forms the basis for spatial modeling to optimize methane drainage borehole trajectories and improve gas capture efficiency. The integrated methodology supports safer mining operations and more effective emission control, and informs future CO_2 storage strategies in post-mining coal seams.

Keywords: well log interpretation, petrophysical parameters, elastic moduli, 1D modeling, coal basins, lithological interpretation

INTRODUCTION

The characterization of petrophysical and geomechanical parameters in the Upper Silesian Coal Basin (USCB) has been widely studied due to their crucial role in understanding rock mass behavior under mining conditions. Geomechanical parameters support mine design and hazard prevention, helping mitigate risks such as excavation instability, roof collapses, and seismic events. Previous studies (e.g., Chudek et al. 2000, Bukowska 2002, 2003, 2006, Bukowska et al. 2012, Moska & Kędzior 2015, Słoczyński et al. 2017, Fryanov 2018, Majkrzak 2019) have improved the understanding

https://doi.org/10.7494/geol.2026.52.2.109 ISSN 2299-8004 | e-ISSN 2353-0790 | Wydawnictwa AGH

of USCB coal seams. Moreover, geomechanical analysis is essential for evaluating coal cuttability, optimizing extraction technologies (Singh et al. 1995, Drzęźla et al. 2000, Sobczyk 2022), and minimizing dynamic geomechanical hazards (Bukowska & Gawryś 2010, Bukowska et al. 2012, Dubiński et al. 2019). A comprehensive characterization of these parameters enables safer and more efficient mining operations, ensuring the protection of both miners and infrastructure. In parallel, petrophysical properties are key to coal seam resource evaluation (Kawęcka 1988). Well log-derived parameters, such as coal density, porosity, and resistivity, are instrumental in distinguishing coal seams from surrounding waste rock (Wood et al. 1983, Ceglarska-Stefańska et al. 1995). Understanding porosity and permeability is particularly critical for assessing coalbed methane (CBM) content and its migration potential, which directly informs methane drainage system designs, which are a key safety measure against methane explosions in Polish coal mines (Prusek et al. 2020). Beyond the mining applications, petrophysical characterization is now being explored for underground carbon dioxide (CO_2) storage in post-mining coal seams supporting sustainable transition strategies (Zarębska & Ceglarska-Stefańska 2006, Wójcicki & Jureczka 2010, Baran et al. 2014). These studies underscore the need for an integrated petrophysical-geomechanical approach to evaluating post-mining utilization scenarios.

A comprehensive assessment of both petrophysical and geomechanical properties can be achieved through well logging data. When calibrated with laboratory measurements, well logs provide continuous depth profiles of rock mass properties, offering a more detailed geological model than traditional seismic surveys. Numerous studies worldwide, particularly in China, Australia, India, and the United States, have leveraged well logs to evaluate coal seam quality and waste rock properties (Fu et al. 2009, Srinaiah et al. 2017, Wood & Cai 2022). However, in Poland, coal characterization has traditionally relied on petrographic studies and laboratory tests, with well log applications remaining underexplored (Wójcicki & Jureczka 2010, Kędzior 2012, Bukowska et al. 2016). To date, no study has comprehensively characterized the Polish part of the USCB by jointly integrating petrophysical and geomechanical parameters based on well-log data. To date, no study has comprehensively characterized the Polish part of the USCB by jointly integrating petrophysical and geomechanical parameters based on well-log data. This gap exists largely because well log-based geophysical surveys have not been widely adopted for mining area characterization. This study focuses on six key boreholes within the USCB – BP-20, BP-21, BP-23, BK-39, KIG-1, and WP-TXA Texaco-A – to develop a robust geological model based on detailed well log interpretation, core sample analysis, and advanced numerical modeling. Apart from these, to better characterize the geomechanical properties of a study area, static mechanical test results from cores collected in 114 underground boreholes were used. These boreholes do not have well log data.

The main objectives are: (1) characterizing the key properties, particularly porosity, permeability, and elastic moduli, (2) evaluating the crucial parameters for methane extraction and mining stability assessments, and (3) linking petrophysical and geomechanical data to improve resource evaluation and hazard mitigation.

GEOLOGICAL SETTING

The study area is located in the southwestern part of the Upper Silesian Coal Basin (USCB), which constitutes a segment of the larger geological unit known as the Upper Silesian Block. This region is characterized by complex tectonics, with numerous faults and folds that significantly influence the distribution and accessibility of coal seams (Fig. 1A) (Buła & Żaba 2008, Buła et al. 2015). The Pniówek coal mine is situated east of the Jastrzębie area, on the southwestern flank of the Main Trough. The area is bounded by two major fault zones: the Jawiszowice fault zone to the north and the Bzie-Czechowice fault zone to the south. The displacement amplitudes in this region reach 400–500 m in the southern part, which further complicates the geological structure (Kotas 1982). The geological structure of the study area comprises Quaternary deposits of Holocene and Pleistocene age, Neogene deposits from the Miocene, and the Upper Carboniferous productive series. The overburden thickness varies from approximately 220 m in the north to around 1,000 m in the south (Jura 2001). A distinct subsidence of the Carboniferous roof toward the south is observed, reaching depths of approximately 1,000 m (Probierz et al. 2012).

Within the Main Trough, the productive Carboniferous sequence has been documented down to a depth of 1,300 m. It includes the Orzesze Beds (Westphalian A) containing coal seams of the 300 series, the Ruda Beds (Namurian C and Westphalian A) with coal seams of the 400 series, and the Saddle Beds (Namurian A and B) comprising coal seams of the 500 series (Fig. 1B). A total of 64 coal seams have been identified in the study area, with an average thickness of 1.33 m, ranging from a minimum of 0.02 m to a maximum of 3.6 m. The productive Carboniferous exhibits a distinct bipartite division, with the lower part representing a paralic series deposited in a marine environment and the upper part consisting of continental (limnic) deposits (Jureczka & Nowak 2016). The Orzesze Beds are dominated by mudstones and claystones, with coal seams occurring mainly within the mudstone layers and less frequently in direct contact with sandstones. The Ruda Beds reach a maximum thickness of 700 m and are subdivided into upper and lower units.

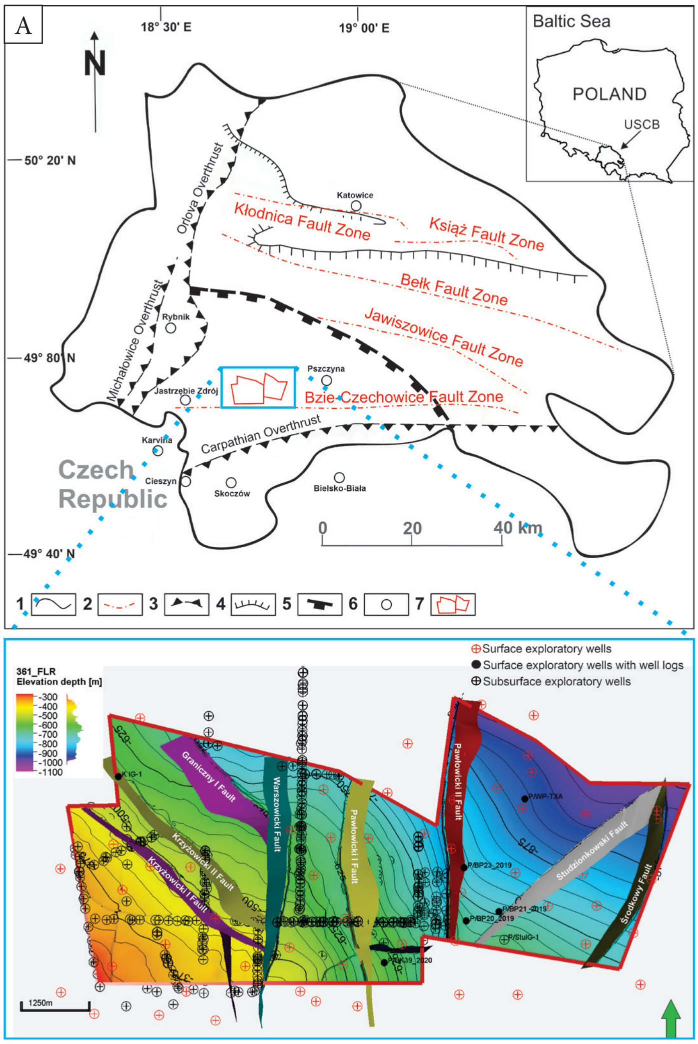

B	STRATIGRAPHY		LITHOSTRATIGRAPHY	
			Series	Beds/average thickness
CARBONIFEROUS	PENNSYLVANIAN (WESTPHALIAN)	MOSCOVIAN	Kraków Sandstone Series	Łaziska Beds/ 457 m
			Mudstone Series	Orzesze Beds
				Załęże Beds/ 102 m
		BASHKIRIAN	Upper Silesian Sandstone Series	Ruda Beds/ 87 m
				Saddle Beds/ 44 m
	MISSISSIPPIAN (NAMURIAN)	SERPUKHOVIAN	Paralic Series	Poruba Beds/ 68 m
				Jakovlec Beds/380 m *
				Hrušov Beds/1300 m*
				Petřkovice Beds/1000 m *

* maximum thickness based on Kotas & Malczyk (1972)

Fig. 1. *Map showing the location of the study area within the USCB (modified after Kędzior 2012) (1 – boundary of the Polish part of the USCB, 2 – important fault zones, 3 – overthrusts, 4 – the range of the continuous Miocene cover, 5 – the range of the secondary methane zone [ticks point the direction inside the areas of ranges], 6 – important cities, 7 – the Pniówek mine boundary), with the zoom on a structural map of the selected coal seam (361) in the study area with borehole locations on the coal mine model (A); the lithostratigraphic division of the productive Carboniferous strata in the USCB with average thickness based on the KIG-1 well (B) (modified after Jureczka & Nowak 2016)*

The Saddle Beds, which occur at significant depths below 1,000 m, display a tendency for seam splitting toward the west and merging toward the east. The average density of coal in this region is 1,380 kg/m^3, ranging from a minimum of 1,130 kg/m^3 to a maximum of 2,150 kg/m^3, which is typical for high-quality coal with a significant degree of coalification. The complex geological structure of the study area, coupled with the lithological diversity and variability in coal seam thickness, presents considerable challenges for coal exploitation due to variability in seam geometry. However, these geological characteristics also provide an interesting subject for petrophysical and geomechanical investigations, especially for assessing the potential of mine methane drainage using horizontal degasification boreholes.

METHODOLOGY

This study employed a systematic interdisciplinary approach, integrating well log analysis, core sample evaluation, and petrophysical modeling. The applied methodologies were designed to extract maximum value from the available data, providing a robust framework for developing a detailed geological model of the Pniówek coal mine in the Upper Silesian Coal Basin. Well log data from six boreholes (BP-20, BP-21, BP-23, BK-39, K IG-1, and WP-TXA) were collected and processed to ensure accuracy and consistency. The intervals of interpretation were 710–1,300 m in the BP-21, BP-23, and BP-39 wells, 560–1,990 m in KIG-1, 310–1,800 m in WP, and 710–1095 in BK-39. The study utilized gamma ray logs (GR) to assess the natural radioactivity of rocks, aiding in lithological identification and multi-well correlation, especially for separating clay-rich units from sandy formations. Borehole diameter was determined using caliper (CALI) logs, which provided insights into borehole wall stability and served as a correction factor for other geophysical measurements. Bulk density (RHOB) was analyzed to estimate porosity and identify lithological variations, including the clear detection of low-density coal seams. Compressional slowness (DT) was measured to evaluate acoustic wave travel time, which was subsequently used to calculate porosity and assess the mechanical properties of the rock formations. Additionally, resistivity logs (LLD and LLS) were employed to determine fluid saturation and identify permeable zones within the geological structure. The raw geophysical data were initially corrected for borehole conditions, including wall roughness and drilling mud invasion, to minimize measurement distortions. Standard normalization techniques were then applied to ensure consistency and allow direct comparison of data across different boreholes. The corrected and normalized datasets were integrated into the Techlog software platform (Schlumberger), facilitating further analysis and interpretation. Apart from deep surface-drilled research boreholes with accompanying well log data, our analyses also included a very large dataset of as many as 114 underground boreholes that lacked well logs but included a rich database of laboratory rock mechanics measurements, aimed at evaluating the rock mass prior to mining activity. An integrated dataset covering a wide spectrum of datasets served as the foundation for a detailed petrophysical and geomechanical characterization of the study area.

Petrophysical modeling

Petrophysical modeling was conducted using the Quanti Elan (QE) module in the Techlog software, a common tool for quantitative interpretation of well log data. The primary objective of this modeling was to determine the volumetric proportions of various mineral constituents, such as clay, coal, quartz, and siderite, as well as to calculate the porosity and permeability of the formation. Siderite was included in the petrophysical model due to its documented presence in the study area, as indicated by numerous core descriptions reporting sideritic concretions. This is also supported by elevated bulk density (RHOB) values, suggesting the occurrence of a relatively dense mineral phase consistent with siderite. The modeling process began with the construction of a mineralogical model, in which a system of linear equations was developed to relate the measured geophysical data to the unknown volumes of rock components. To optimize the model, the least-squares method was applied, minimizing the difference between the measured and synthetic well log responses. The model calibration was performed using laboratory measurements of core samples, providing an independent estimate of porosity and permeability. This step ensured that the model reflected the formation conditions. Based on the calibrated model, the volumetric proportions of individual mineral constituents were determined, along with the effective porosity (Phi) and permeability (K).

Rock type identification

Rock types with distinct petrophysical properties were identified through a detailed analysis of cross-plots, which graphically represent relationships between different parameters. In this study, cross-plots of clay volume (Vcl) versus coal volume (COAL_QE) and Vcl versus the sum of Quartz_QE and Siderite_QE volumes were utilized to distinguish between different rock types. As a result, five distinct rock types were identified: coal, shale coal, clean sandstone, shaly sandstone, and mudstone. These rock types were further analyzed to determine their specific petrophysical and mechanical properties, such as porosity, permeability, and elastic moduli. Identifying rock types was essential for understanding formation heterogeneity and making accurate predictions regarding reservoir quality and mechanical behavior.

The classification was initially performed through interactive selection on the cross-plots. Once predefined, the rock type classes were propagated to other wells using the hierarchical tagging method in the Techlog software. The heterogeneous rock analysis (HRA) tagging process involved applying the HRA_Class generated in the clustering module to designated wells within the tagging module. It involves assigning individual data points (e.g., log measurements) to predefined lithologic classes based on multidimensional data space, often after preprocessing or dimensionality-reduction steps.

Additionally, linear discriminant analysis (LDA) was employed to transform input data into a coordinate system that maximized the separation of class centroids. It is a supervised statistical classification technique that identifies linear combinations of variables that best separate predefined groups. It is commonly used to classify rock types or petrophysical trends in geoscience and petrophysics (Fisher 1936). The classification process relied on either pooled or class-specific covariance matrices to assign new prediction data to the appropriate rock type class. Unlike principal component analysis (PCA), which was used in the clustering to maximize variance discrimination, the LDA focused specifically on optimizing class separation in the tagging phase (Doveton 1994). It is an unsupervised dimensionality-reduction method that transforms the original variables into a set of principal components capturing the maximum variance in the dataset. PCA is widely applied in petrophysical analysis to identify trends, clusters, or correlations among well-log measurements (Pearson 1901, Murariu et al. 2025, Ye 2025)

Permeability calculation

Permeability, a key parameter for evaluating fluid flow within subsurface formations, was estimated using empirical formulas derived from laboratory measurements on core samples. These relations, which establish relationships between porosity and permeability for each rock type, were applied to the well log data to generate continuous permeability logs along the boreholes. The permeability of different rock types exhibited significant variability. Coal demonstrated the highest permeability values, primarily due to their higher porosity and natural fracturing. High permeability facilitates fluid movement. In contrast, sandstones, despite their relatively high porosity, exhibited lower permeability, likely due to their compact and cemented structure, which restricts fluid flow. The empirical formulas for the permeability estimation were obtained from laboratory-core-measured porosity and permeability. The resulting permeability profiles were then analyzed to identify potential zones of enhanced fluid flow, which could act as pathways for methane migration or targets for enhanced recovery techniques.

Methodology of laboratory measurements on core samples

The mechanical parameters were determined using MTS-810 and MTS-815 testing machines, in accordance with the applicable testing procedures developed based on the Polish PN-G-04303 standard. The uniaxial compressive strength (Rc) was measured on air-dried specimens using regular-shaped samples. The testing method involved loading regular rock specimens in the form of cylinders or rectangular prisms, in accordance with the standard PN-G-04303:1997. Tensile strength (Ts) was determined via the Brazilian test. In accordance with the Polish PN-G-04302:1997 standard, the elastic parameters, including Young's modulus, were determined using the BL-3/ZLGIG/PB-03 procedure. The value of the internal friction angle was obtained using the strength parameters in accordance with the PN-81/B-03020-3 standard. Grain density was measured using a Micromeritics AccuPyc 1340 helium pycnometer, which exploits helium's ability to penetrate submicropores. Bulk density was determined with a Micromeritics GeoPyc 1360 analyzer using quasi-fluid pycnometry. These measurements were used to calculate the helium porosity (PHI). Permeability was measured mainly with a Corelab PDP-250 pulse-decay permeameter for tight rock samples (from 10 nD to 1 mD), using nitrogen at a test pressure of 2,000 psi (this pressure corresponds to the anticipated in situ reservoir conditions) and a confining pressure of 5,000 psi. Samples were dried at 110°C for 24 hours before analysis. For sandstones with porosity above 10%, permeability was measured using TEMCO equipment under a steady-state nitrogen flow, applying Darcy's law in a linear flow geometry through cylindrical core plugs 1 inch in diameter and 3–4 cm in length.

Elastic properties estimation

Before the static values can be estimated, the dynamic values are calculated from well log data. Due to a lack of shear slowness (DTS) data, the DTS values were calculated with the use of the Castagna model according to Equation (1):

$$V_s = \left(\sum_i \frac{V_{fi}}{a_i V_p^2 + b_i V_p + c_i} \right)^{-1} + \sum_i V_{fi} \left(a_i V_p^2 + b_i V_p + c_i \right) \quad (1)$$

where: V_p and V_s are the compressional and shear wave velocities for brine-saturated rocks [m/s], a_i, b_i, c_i are the empirical coefficients determined for the specific rock types, and V_{fi} represents the volume fractions of specific minerals, including quartz and clay minerals [v/v].

The dynamic elastic moduli of the reservoir (Young's modulus – E and Poisson's ratio – PR) were calculated based on the measured compressional slowness (DTP) and bulk density (RHOB) and the calculated values of shear slowness (V_s):

$$\mathrm{E} = \mathrm{RHOB} \times V_s^2 \times \frac{\left(3V_p^2 - 4V_s^2\right)}{\left(V_p^2 - V_s^2\right)} \quad (2)$$

$$\mathrm{PR} = \frac{V_p^2 - 2V_s^2}{2\left(V_p^2 - V_s^2\right)} \quad (3)$$

where: RHOB – bulk density obtained from well logs [g/cm^3], V_p – P-wave velocity derived from the DTP logs [m/s], and V_s – S-wave velocity estimated using Castagna's formula [m/s].

Estimated static elastic properties are essential for geomechanical modeling and designing safe mining operations, ensuring accurate predictions of rock behavior under stress conditions and reservoir characterization. To obtain continuous static values of E and PR, laboratory-measured static values were used to develop continuous E and PR logs along the boreholes, improving the accuracy of the geomechanical assessments. Table 1 presents the relationships between static (E_stat) and dynamic (E_dyn) values of Young's modulus and Poisson's ratio (PR_stat vs. PR_dyn). These equations provided conversion functions, allowing dynamic log-derived values to be transformed into their static equivalents in the entire borehole profile. It should be emphasized that this relationship is not a classical statistical correlation, but rather an empirical relation that makes it possible to obtain continuous curves of static elastic parameters.

Table 1
Relationships between static and dynamic values of Young's modulus and Poisson's ratio

Rock types	Relation
Relationship between E_stat and E_dyn	
Sandstone	E_stat = 0.14·E_dyn + 6.04
Other rock types	E_stat = 0.15·E_dyn + 2.045
Relationship between PR_stat and PR_dyn	
All rock types	PR_stat = 0.88·PR_dyn − 0.15

RESULTS AND DISCUSSION

Porosity and permeability distribution

A total of 112 laboratory core measurements of permeability and porosity were performed in well BDK-105. Additionally, 31 core measurements of vertical permeability in sandstones were conducted in this wellbore. The laboratory-measured porosity distributions across different rock types varied significantly. The highest porosity values were observed in the sandstone, ranging from 8.7 to 12.3%, which is consistent with its well-sorted nature, allowing for the development of substantial pore space. However, despite the relatively high porosity, the permeability of these sandstones was lower than expected, particularly in the more compacted or cemented intervals. This indicates that permeability is not solely controlled by porosity but is also influenced by factors such as grain size, sorting, and degree of cementation. The presence of kaolinite-illite cement and compaction likely reduces the pore connectivity, leading to restricted fluid flow.

In contrast, the laboratory-measured values of permeability in the coal exhibited the highest values despite their lower porosity. The permeability of the coal ranged from 0.2 to 2 mD, significantly exceeding that of the surrounding sandstones and mudstones. The two circled black data points for coal (Fig. 2A) represent samples that were damaged (cracked) during laboratory measurements, which affected the reliability of the obtained values, as their permeability reached values close to 1 mD. Consequently, these points were excluded from the regression analysis. This elevated permeability of coal is attributed to the presence of fractures and cleats, which enhance pore connectivity and facilitate fluid migration. On the other hand, shale-coal, which contains a mixture of coal and shale, exhibits much lower permeability due to the compact nature of the formation. The mudstones, characterized by high clay content and low porosity, demonstrated the lowest permeability values, functioning as effective sealing layers capable of trapping gas within coal seams.

The cross-plots of porosity versus permeability (Fig. 2) provide a detailed visualization of these relationships, illustrating the variability across different rock types and boreholes. The empirical equations used to estimate the permeability from the porosity (Table 2) were found to be generally accurate, though some deviations were observed in more heterogeneous or fractured intervals.

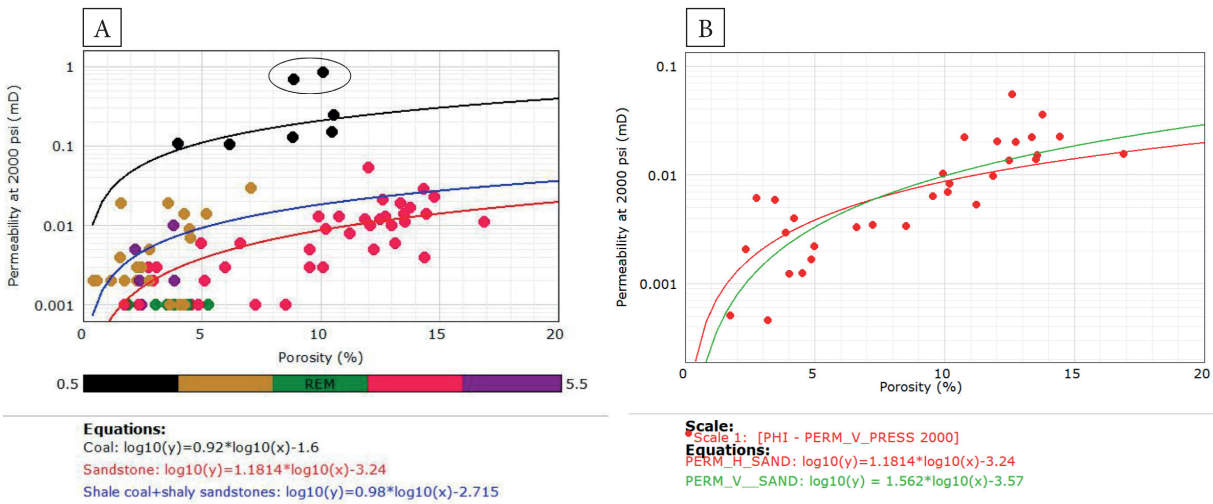

Fig. 2. *Porosity and permeability characteristics of studied rock types: A) relationship between laboratory-measured horizontal permeability and porosity at 1,500 psi of pressure; color scale refers to lithology: black – coal, violet – shale coal, brown – shaly sandstones, green – mudstones and claystones, pink – sandstones; the colorful lines describe the relationship between permeability and porosity for different rock types; B) the green line shows the relationship between porosity and vertical permeability for sandstones, while the red line is the relationship between porosity and horizontal permeability for sandstones (as in Figure 2A) for comparison*

Table 2
Empirical equations for permeability estimation based on porosity for different rock types. For sandstones, both the vertical PERM_V and horizontal PERM_H permeability were calculated

Rock type	Name of variable	Equation
Coal	PERM1	$\log_{10}(\text{PERM1}) = 0.92 \cdot \log_{10}(\text{PHI}) - 1.6$
Shaly sandstones and coal shales	PERM2	$\log_{10}(\text{PERM2}) = 0.98 \cdot \log_{10}(\text{PHI}) - 2.715$
Mudstones and claystones	PERM3	$(\text{PERM2} + 0.001)^{0.5}$
Sandstones	PERM_H	$\log_{10}(\text{PERM\_H}) = 1.19 \cdot \log_{10}(\text{PHI}) - 3.24$
Sandstones	PERM_V	$\log_{10}(\text{PERM\_V}) = 1.562 \cdot \log_{10}(\text{PHI}) - 3.57$

These discrepancies suggest that additional factors, such as natural fractures or localized cementation variations, may play a role in controlling permeability and should be considered in future studies. Table 3 presents the equations used for permeability estimation based on porosity for different rock types. For coals, permeability follows a logarithmic trend, while for sandstones, a steeper dependency on porosity is observed. Notably, sandstones exhibit comparable permeability values in both the horizontal and vertical directions, indicating isotropic characteristics. The data in Table 3 (summary of average porosity and permeability values for different rock types) confirm the very low permeability of sandstones, comparable to that of mudstones and clays.

Despite their average porosity of nearly 9%, the sandstones are highly compacted, reducing fluid flow pathways. Although the matrix of these rocks is nearly impermeable, stress relief episodes associated with coal excavations may have enhanced the permeability in some areas. According to Kędzior (2012), the permeability of mudstone sequences in the Orzesze and Załęże formations may reach up to 242 mD in sandstones (Krzanowska 2002). Furthermore, permeability measurements conducted at 1,500 psi and 2,000 psi closely reflect reservoir conditions. In the K IG-1 well, the permeability values align with formation pressures, ranging from 1,000 psi at 640 m depth in the Załęże Beds to 3,119 psi at 1,998 m depth in the Saddle and Poruba beds.

The low sandstone permeability under these pressures indicates that compaction and diagenetic cementation have strongly reduced the reservoir quality. Table 4 summarizes the average reservoir and elastic properties for each rock type. The clay, quartz, siderite, and coal volumes were also analyzed to assess their contribution to the petrophysical properties of the reservoir. Two outlier samples in Figure 2 exhibited permeability values exceeding 1 mD, which deviates from the established porosity–permeability trend. These anomalies may result from fractures, although it remains uncertain whether these fractures formed *in situ* or during sample transportation and laboratory handling. Consequently, these high-permeability coal samples were excluded from the development of the PHI vs. PERM relationship to ensure consistency in permeability modeling.

Table 3
Summary of average porosity and permeability values for different rock types

Rock type	Arithmetic mean of porosity [%]	Geometric mean of permeability H 1,500 psi [mD]	Geometric mean of permeability H 2,000 psi [mD]	Geometric mean of permeability V 2,000 psi [mD]
Coal	9.33	0.3810	0.227	unavailable
Coal shale	2.88	0.0030	0.003	no data
Mudstones and clays	2.99	0.0038	0.003	no data
Shaly sandstones	no data	no data	no data	no data
Sandstones	8.92	0.0070	0.006	0.006

H – horizontal, V – vertical.

Table 4
Average reservoir and elastic properties for each rock type in the selected boreholes

Well name	Average clay volume [v/v]	Average porosity [v/v]	Average permea-bility [mD]	Average quartz fraction [v/v]	Average siderite fraction [v/v]	Average coal fraction [v/v]	Average Young's modulus (static) [GPa]	Average Poisson's Ratio (static) [–]
Coal								
BK-39	0.192	0.083	0.176	0.02	0.029	0.675	2.366	0.165
BP-20	0.156	0.054	0.118	0.095	0	0.695	2.877	0.162
BP-21	0.180	0.091	0.191	0.081	0	0.648	2.732	0.157
BP-23	0.133	0.095	0.198	0.079	0.006	0.687	3.113	0.173
K-1	0.242	0.104	0.217	0.026	0	0.627	3.360	0.224
WP-TXA	0.173	0.125	0.257	0.064	0.004	0.635	1.591	0.177
Average	0.179	0.092	0.188	0.061	0.007	0.661	2.673	0.176
Coal shale								
BK-39	0.433	0.082	0.012	0.137	0.034	0.313	3.856	0.126
BP-20	0.409	0.078	0.011	0.193	0.002	0.319	4.407	0.133
BP-21	0.358	0.102	0.015	0.234	0.006	0.301	3.707	0.135
BP-23	0.370	0.090	0.013	0.225	0.018	0.296	4.128	0.149
K-1	0.448	0.083	0.012	0.135	0.004	0.331	3.971	0.168
WP-TXA	0.408	0.091	0.013	0.171	0.015	0.316	3.312	0.137
Average	0.404	0.088	0.013	0.183	0.013	0.313	3.897	0.141
Shaly sandstones								
BK-39	0.422	0.053	0.007	0.427	0.094	0.004	8.611	0.054
BP-20	0.368	0.056	0.008	0.479	0.080	0.018	8.808	0.070
BP-21	0.395	0.062	0.009	0.466	0.074	0.004	7.880	0.065
BP-23	0.398	0.054	0.007	0.455	0.069	0.023	8.305	0.070
K-1	0.387	0.047	0.006	0.49	0.060	0.015	8.098	0.062
WP-TXA	0.414	0.054	0.007	0.436	0.059	0.038	9.036	0.058
Average	0.397	0.054	0.007	0.459	0.073	0.017	8.456	0.063
Mudstones and clays								
BK-39	0.521	0.058	0.003	0.339	0.073	0.009	7.410	0.071
BP-20	0.500	0.061	0.003	0.337	0.067	0.036	8.024	0.083
BP-21	0.513	0.068	0.003	0.342	0.069	0.007	7.106	0.081
BP-23	0.512	0.056	0.003	0.350	0.056	0.026	7.385	0.087
K-1	0.538	0.046	0.002	0.343	0.047	0.027	6.472	0.098
WP-TXA	0.527	0.061	0.003	0.328	0.049	0.035	7.113	0.084
Average	0.519	0.058	0.003	0.340	0.060	0.023	7.252	0.084
Sandstones								
BK-39	0.242	0.091	0.008	0.594	0.063	0.009	12.440	0.046
BP-20	0.176	0.089	0.008	0.645	0.073	0.017	12.491	0.068
BP-21	0.245	0.090	0.008	0.593	0.068	0.005	12.336	0.051
BP-23	0.226	0.084	0.007	0.593	0.068	0.029	12.768	0.056
K-1	0.269	0.077	0.006	0.578	0.065	0.011	16.065	0.046
WP-TXA	0.162	0.086	0.007	0.611	0.045	0.097	13.465	0.041
Average	0.220	0.086	0.007	0.602	0.064	0.028	13.261	0.051

Geomechanical properties based on laboratory data from underground boreholes

Mechanical properties, such as unconfined compressive strength (Rc), tensile strength (Ts), Young's modulus (E), Poisson's ratio (PR), and friction angle (FA), are fundamental for evaluating the stability and mechanical performance of the rock mass in coal mining contexts. These properties determine how different rock types respond to stress, ensuring safe mining practices and effective excavation techniques. To characterize the mechanical properties and examine the relationships between specific strength and elastic parameters, we combined laboratory-derived static mechanical test results obtained from cores from a group of 114 underground boreholes (Rc, Ts, and FA) with elastic properties (Young's modulus E), for the four rock types present in the study area.

The dataset shown in Figure 3, plotted for mudstones and clays (A), shaly sandstones (B), sandstones (C), and coal (D), indicates that the coal exhibits significantly lower strength and rigidity than the other rock types, with Rc values up to 18.08 MPa and E values up to 2.1 GPa. This is primarily due to its high organic content and cleat structure, which makes it more susceptible to deformation (Ranjith & Perera 2012). In contrast, shales and shaly sandstones exhibit moderate Rc and E values, with Rc reaching 101 MPa in shaly sandstones and 124 MPa in shales, while their maximum E values are 16 GPa and 22 GPa, respectively. Sandstones display the highest mechanical strength, with Rc values up to 158 MPa and E reaching 23 GPa, which can be attributed to their granular structure and high quartz content, making them strong and rigid. A positive correlation between Rc and E is observed across all rock types, suggesting that an increase in compressive strength (Rc) corresponds with a rise in Young's modulus (E), enhancing the rock's resistance to deformation (Li et al. 2019). However, the degree of correlation varies among rock types due to differences in mineral composition and internal structure (Chang et al. 2006).

The relationship between unconfined compressive strength (Rc) and friction angle (FA) for different rock types is illustrated in Figure 4.

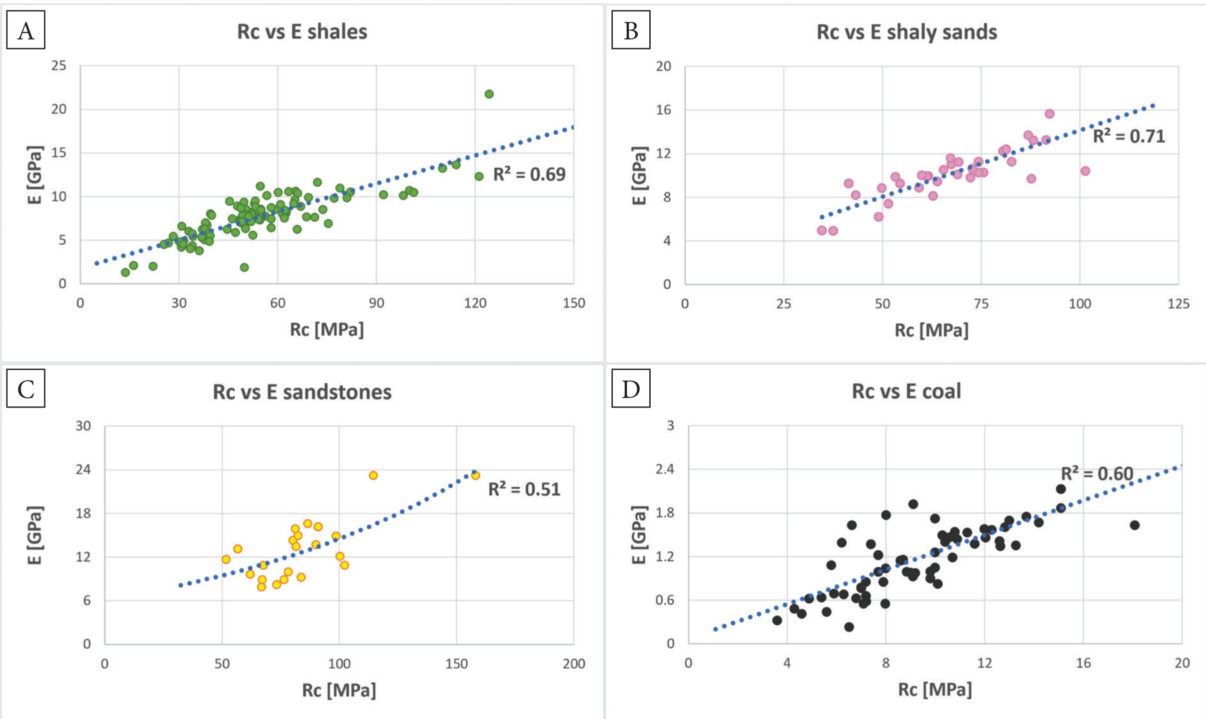

***Fig. 3.** Cross-plots showing the relationship between unconfined compressive strength (Rc) and Young's modulus (E) for different rock types: shales (A), shaly sandstones (B), sandstones (C), and coal (D)*

The results show that sandstones exhibit the strongest correlation between Rc and FA, with $R^2 = 0.97$, reflecting their high grain interlocking and quartz-dominated composition. Shales and shaly sandstones demonstrate moderate strength, but their friction angle is limited by the clay content, which weakens the rock's internal cohesion. Coal exhibits the lowest Rc and FA values, primarily due to its high organic matter content and cleat structure, which makes it the least rigid rock type. A strong positive correlation between Rc and FA is observed across all rock types, indicating that as the compressive strength increases, the rock's resistance to shear failure also increases due to stronger internal bonding and reduced pore space (Xie et al. 2023). Due to the lack of porosity measurements on rock samples from boreholes drilled in coal seams, the effect of porosity on mechanical properties was not analyzed in this study.

Unconfined compressive strength (Rc) represents the maximum stress a material can withstand in compression, while tensile strength (Ts) measures its resistance to tension. Generally, rocks exhibit much lower tensile strength than compressive strength due to weaker bonding under tension, making them more prone to fracturing (Song et al. 2024). The Rc/Ts ratios for the analyzed rock types are presented in Table 5. The results indicate that non-coal rock types exhibit Rc/Ts ratios ranging from 6–7 (minimum) to 18–30 (maximum) for sandstones and shaly sandstones. Coal has significantly higher Rc/Ts ratios, with a minimum of 27 and a maximum of 56, reflecting its heterogeneous structure and low tensile strength. Such ratios confirm coal's mechanical anisotropy and fracture-prone behavior. Shales have the highest Rc/Ts ratio, reaching up to 109, due to their laminated structure and weak bedding planes (Xie et al. 2023, Małkowski & Niedbalski 2024). A moderate correlation between Rc and Ts is observed across all rock types, with R^2 values between 0.54 and 0.57 (Fig. 5). Although a general trend exists where a higher UCS (unconfined compressive strength) corresponds to a higher tensile strength, the relationship is not particularly strong due to pre-existing fractures, bedding planes, and structural variations (Rybacki et al. 2015, Li et al. 2019).

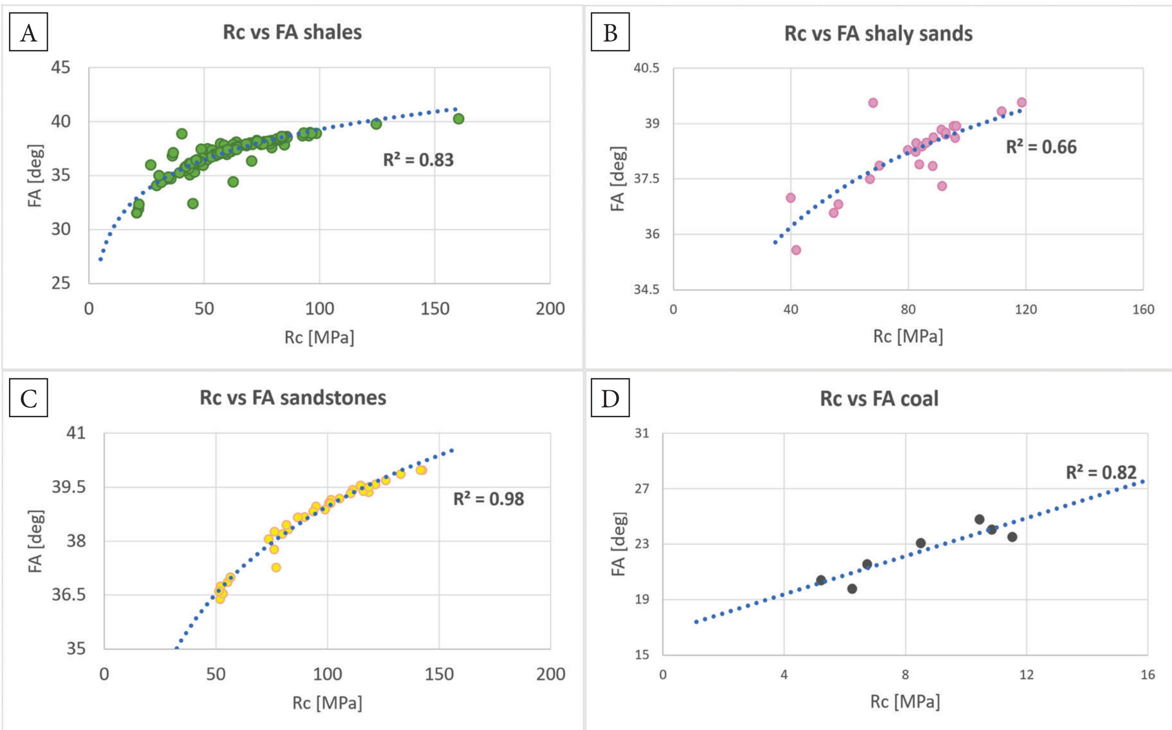

Fig. 4. *Cross-plots illustrating the correlation between unconfined compressive strength (Rc) and friction angle (FA) for different rock types: shales (A), shaly sandstones (B), sandstones (C), and coal (D)*

Table 5
Statistical characteristics of the ratio between uniaxial compressive strength (Rc) and tensile strength (Ts) for different rock types

Rc and Ts ratio	Mudstones and clays	Shaly sandstones	Sandstones	Coal
Average value	17.46	16.00	11.97	39.11
Min value	6.59	7.30	7.46	27.00
Max value	109.09	30.33	18.85	55.93
Stand. dev.	14.10	7.23	3.00	8.15

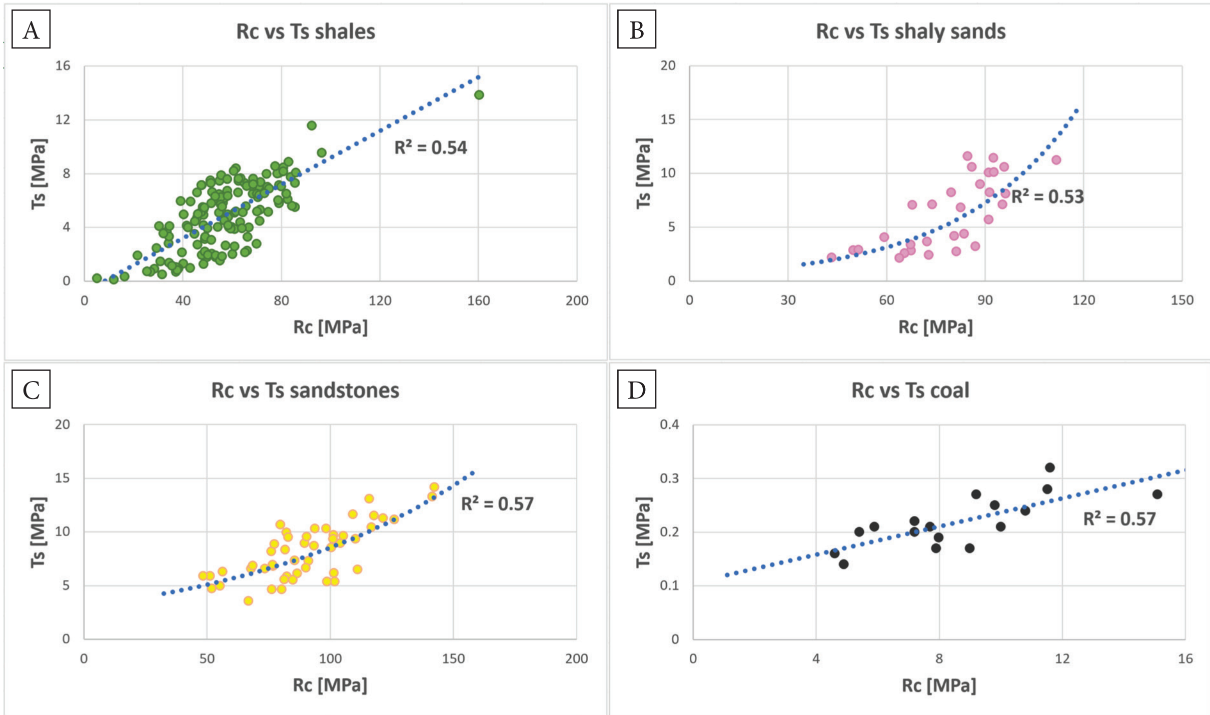

Fig. 5. *Cross-plots depicting the relationship between unconfined compressive strength (Rc) and tensile strength (Ts) for different rock types: shales (A), shaly sandstones (B), sandstones (C), and coal (D)*

Among all rock types, sandstones exhibit the highest tensile strength, indicating better grain bonding and structural integrity under tension, whereas coal shows the lowest Ts values due to its weak cleat structure. Empirical correlation functions with coefficients of determination (R^2), describing the relationships between the above-outlined mechanical properties, are listed in Table 6.

The elastic properties of the analyzed formations, represented by Young's modulus (E), differ significantly among rock types, reflecting variations in mechanical behavior and stability. Coals have the lowest E values, ranging from 1.2 to 1.5 GPa, indicating low stiffness and high susceptibility to deformation. This aligns with their petrophysical characteristics, making them more prone to compaction and subsidence during gas extraction. Conversely, sandstones show higher E values (8–13 GPa), indicating greater rigidity and resistance to deformation. Their high modulus is due to their compact and cemented structure, which enhances stability and reduces subsidence risk.

Table 6
Empirical correlation functions and their coefficients of determination (R^2) describing the relationships between key mechanical properties – unconfined compressive strength (Rc), Young's modulus (E), friction angle (FA), and tensile strength (Ts) – for the analyzed rock types: shales, shaly sandstones, sandstones, and coal

Rock type	Shales	Shaly sandstones	Sandstones	Coal
Rc versus E				
Regression function	$y = 0.1078x + 1.8017$	$y = 0.1217x + 1.9794$	$y = 6.1709e^{0.0086x}$	$y = 0.1188x + 0.073$
Coefficient of determination R^2	0.6874	0.7059	0.5104	0.6051
Rc versus FA				
Regression function	$y = 4.043 \ln(x) + 20.655$	$y = 2.8978 \ln(x) + 25.514$	$y = 3.5061 \ln(x) + 22.819$	$y = 0.687x + 16.633$
Coefficient of determination R^2	0.8331	0.6576	0.9766	0.8236
Rc versus Ts				
Regression function	$y = 0.0998x - 0.787$	$y = 0.5829e^{0.028x}$	$y = 3.0428e^{0.0103x}$	$y = 0.0131x + 0.1056$
Coefficient of determination R^2	0.5441	0.5393	0.5662	0.5676

Static versus dynamic elastic properties

Dynamic E and PR values are generally higher than static values, which can overestimate formation stiffness, especially in coals. This discrepancy underscores the importance of calibrating dynamic measurements using laboratory data, as only static values are used for stability assessments during mining operations. The results for the K IG-1 well are shown in Figure 6. Track 2 shows dynamic and static PR, and Track 3 shows dynamic and static E. These values were calibrated using laboratory measurements (black dots). In track 4, the lithological rock types identified in the K IG-1 borehole are distinguished by different colors: coal is marked in black (W), coal shales in purple (WZL), mudstones and clays in green (IL), shaly sandstones in brown, and sandstones in yellow (PSC). This classification aids in understanding the variation in elastic properties across different geological units. The correlation between static Young's modulus (E_stat) and static Poisson's ratio (PR_stat) is summarized in Table 7. The results indicate a strong negative correlation, with higher PR values generally associated with lower E values. This relationship is particularly evident in shaly sandstones and mudstones, where the presence of clay minerals significantly reduces stiffness. The equations presented in Table 7 describe the empirical dependence of E_stat on PR_stat for different rock types. The coefficients of determination (R^2) suggest a strong correlation for most rock types, with values ranging from 0.497 to 0.845, confirming the robustness of these regression models. These findings highlight the necessity of incorporating static elasticity measurements in geomechanical modeling to enhance the accuracy in predicting deformation and subsidence risks in underground coal seams. The presented regression equations can be employed in future studies to estimate static elastic parameters for formations where direct laboratory measurements are unavailable.

Table 7
Empirical relationships between static Young's modulus (E_stat) and static Poisson's ratio (PR_stat) for different rock types

Rock type	Relationship between E_stat and PR_stat	*R*	R^2
Coal	$\log_{10}(E\_stat) = -2.605 \cdot PR\_stat + 0.832$	−0.705	0.497
Coal shales	$\log_{10}(E\_stat) = -3.369 \cdot PR\_stat + 1.036$	−0.862	0.742
Mudstones and clay	$\log_{10}(E\_stat) = -3.974 \cdot PR\_stat + 1.171$	−0.919	0.845
Shaly sandstones	$\log_{10}(E\_stat) = -3.830 \cdot PR\_stat + 1.155$	−0.916	0.839
Sandstones	$\log_{10}(E\_stat) = -2.312 \cdot PR\_stat + 1.228$	−0.910	0.827

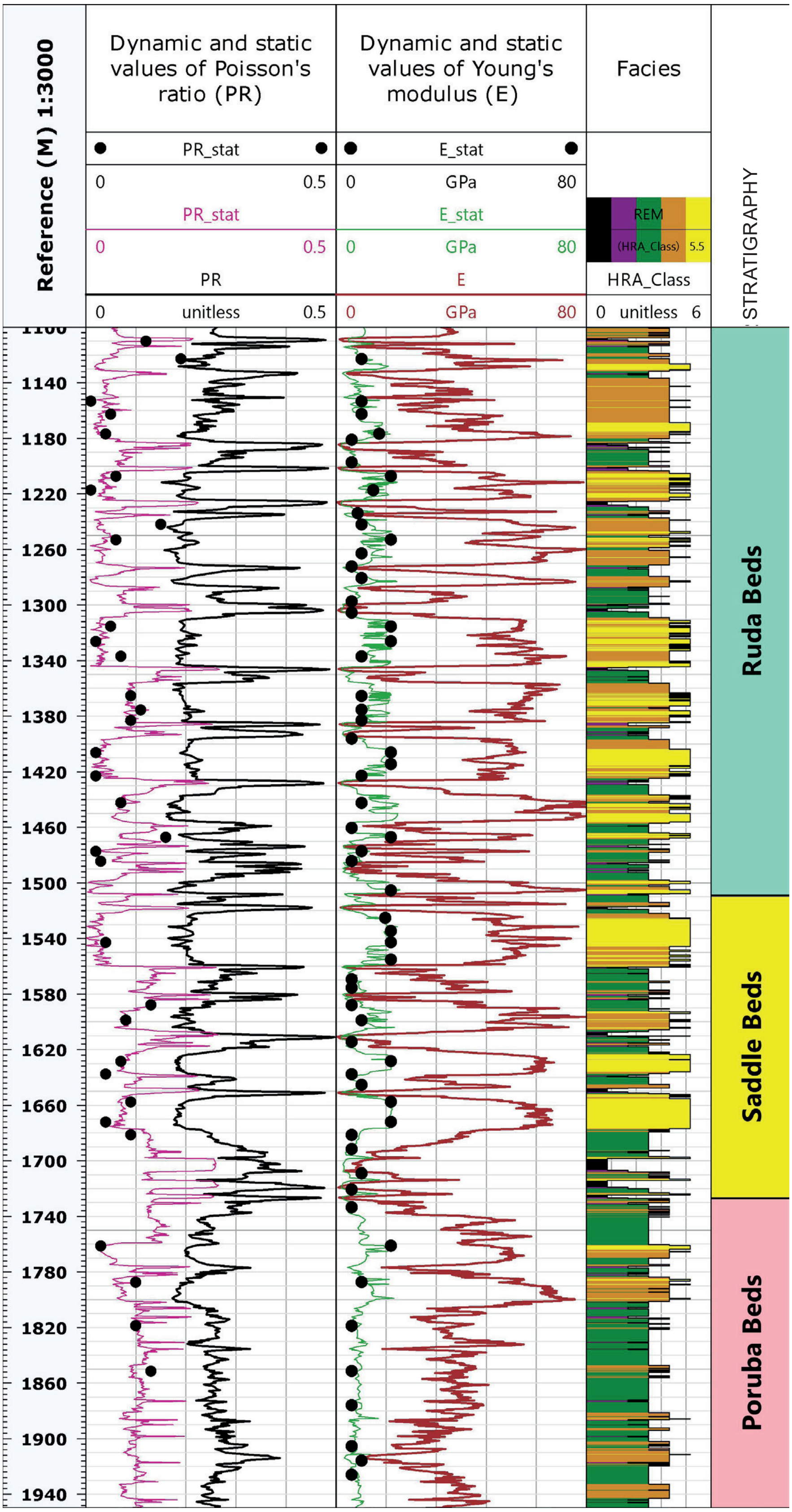

Fig. 6. *Interpretation of elastic properties in the KIG-1 borehole, including static and dynamic Young's modulus (E) and Poisson's ratio (PR), calibrated with laboratory data (black dots)*

Characteristics of the rock types within the lithostratigraphic beds

The results of petrophysical and geomechanical wellbore interpretation in six wells (Fig. 7 on the interleaf) cover depths from a few hundred meters to approx. 1,000 m. The Załęże Beds are primarily composed of fine-clastic deposits, including mudstones and siltstones, which have been confirmed to act as effective sealing formations. Their low permeability and high clay content create an excellent barrier to fluid migration, which is crucial for trapping methane within the underlying coal seams. A laminar, carbonaceous microtexture further improves the sealing by reducing the permeability. The Ruda and Saddle beds exhibit a more complex lithological and petrophysical character, primarily due to their higher quartz content and kaolinite-illite cement. These formations are dominated by coarse- and medium-grained sandstones, which exhibit moderate porosity, particularly in cleaner, better-sorted intervals. However, the presence of detrital clay and other impurities within the sandstones significantly reduces the permeability, especially in poorly sorted or highly cemented zones.

The variability in mineral composition and grain sorting suggests deposition in a dynamic, high-energy environment, potentially influenced by fluvial or shallow marine processes. The occurrence of well-rounded to subangular grains, combined with a micro-directional texture characterized by mica laminae and pelitic siderite, indicates that these beds underwent significant reworking, either through multiple cycles of deposition and erosion or under the influence of strong currents during sedimentation. The Poruba Beds, representing the paralic series, exhibit considerable lithological heterogeneity, reflecting the cyclic nature of their deposition. The alternation between clastic and phytogenic sediments, with varying proportions of sandstones, mudstones, and coal seams, suggests deposition in a coastal or deltaic environment, where fluctuations in sea level or sediment supply led to periodic shifts in the depositional regime. Coal seams and strong lithological variability make this unit important for methane extraction. The thin coal seams, typically ranging from 1 to 1.5 m in thickness, are interbedded with fine- to medium-grained sandstones, which constitute 20–50% of the entire series. This architecture forms a dual system: coal as the main reservoir and sandstones as secondary migration pathways. The coal-bearing horizons of the Saddle Beds exhibit the lowest clay content compared to the Ruda and Załęże beds, along with the highest porosity, exceeding 10%, and permeability values reaching approximately 0.25 mD. The coal volume varies between 68% in the Saddle Beds and 65% in the Załęże Beds, whereas no coal seams are observed within the Poruba Beds. Coal shales, on the other hand, exhibit significantly lower permeability compared to coals, with values ranging from 0.01 to 0.012 mD. The highest coal volume is found in the Saddle Beds (37%), whereas the Poruba Beds contain the highest clay volume (51%). The mudstone and claystone sequences of the Poruba Beds contain the highest clay fraction (60%) and an average permeability of approximately 0.1 mD. The porosity of the mudstones decreases with depth, from 6.3% in the Załęże Beds to 2.2% in the Poruba Beds. Additionally, a coal fraction of 1–2.8% is observed within the mudstone series. The porosity of the sandstones averages 9.1% in the Załęże Beds, decreasing with depth to 4.3% in the Poruba Beds. The clay fraction within the sandstone series is relatively consistent, ranging from 20% to 22%, with the highest values observed in the Poruba Beds (up to 30%). A minor coal admixture is present within the Saddle Beds (5%) and the Załęże Beds (4%). The permeability of the sandstones is very low in both horizontal and vertical directions, indicating the isotropic nature of the sandstone series.

Laboratory-measured permeability values range from 0.008 mD in the Załęże Beds to 0.003 mD in the Poruba Beds. Shaly sandstones, characterized by a higher shale fraction (ca. 40%) and lower porosity, exhibit porosity values ranging from 5.8% in the Załęże Beds to 1.8% in the Poruba Beds. Their permeability is also low, decreasing from 0.007 mD in the Załęże Beds to 0.002 mD in the Poruba Beds.

The petrophysical characteristics of individual rock types within the studied lithostratigraphic beds are summarized in Figure 8.

The histograms (Fig. 8) illustrate the distribution of average parameter values and highlighting key trends. A comprehensive summary of the average mineral composition, reservoir properties, and elastic parameters for different rock types and stratigraphic beds is provided in Table 8, facilitating a comparative analysis of the variability in rock properties across the study area. The highest Young's modulus values are found in the sandstones of the Poruba Beds (15.9 MPa) and the Saddle Beds (15.5 MPa). The lowest values are observed in coals (2.2–2.7 MPa). Coal shales of the Poruba Beds exhibit higher Young's modulus values (5.5 MPa) compared to those in the Załęże Beds (3.9 MPa) and the Saddle Beds (3.3 MPa). The Young's modulus values for mudstones remain relatively consistent, ranging from 7 MPa in the Poruba Beds to 7.3 MPa in the Ruda Beds. The highest Poisson's ratio values are observed in the coals of the Saddle Beds (0.21), followed by the coal shales of the Poruba Beds (0.185) and the Saddle Beds (0.17). The variation in Young's modulus (*E*) and Poisson's ratio (PR) among different rock types within the Załęże, Ruda, Saddle, and Poruba beds is depicted in Figure 9.

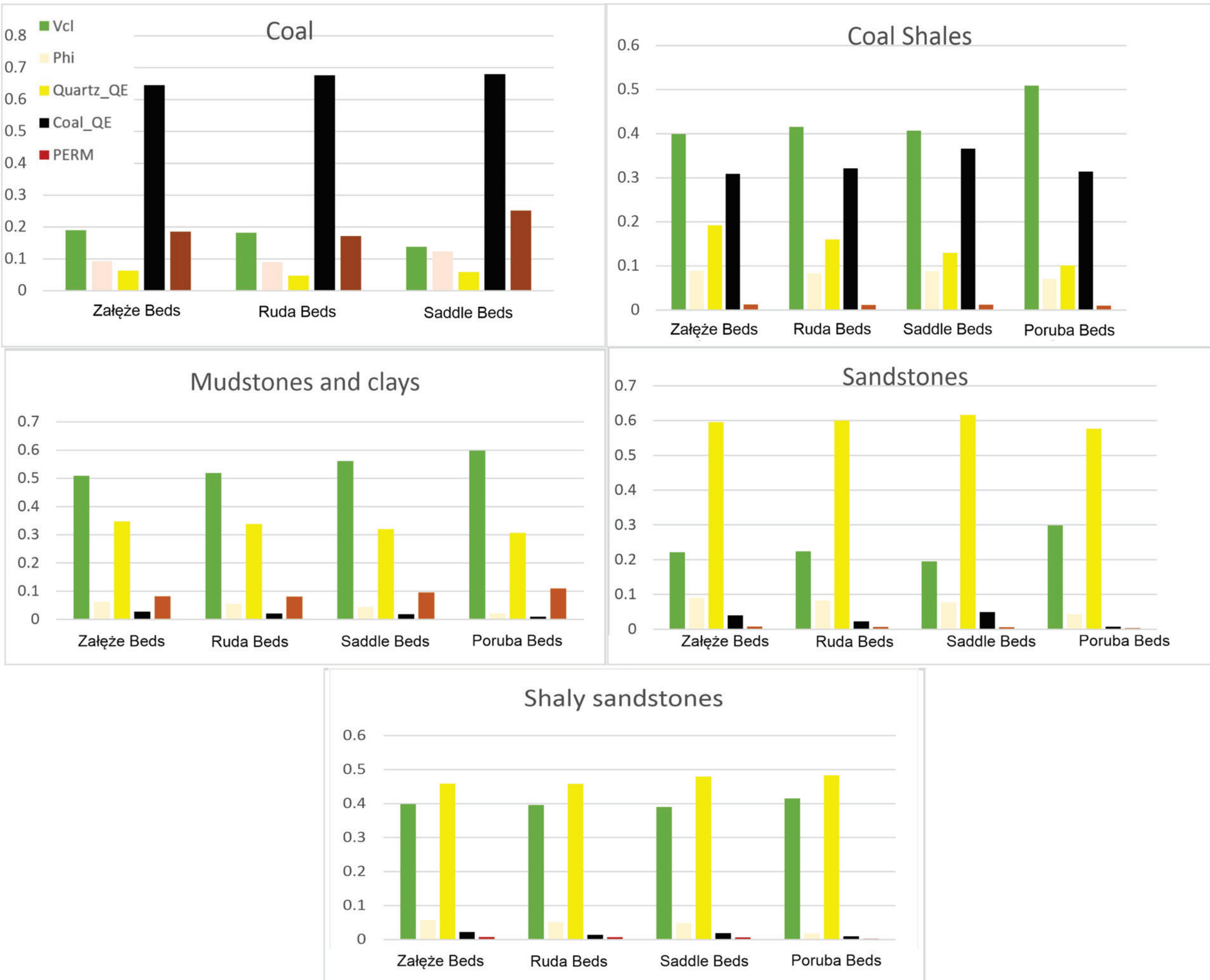

Fig. 8. *Distribution of selected petrophysical and mineralogical parameters (Vcl, porosity (Phi), quartz content (Quartz_QE), coal content (Coal_QE), and permeability (PERM)) for different lithologies and stratigraphic units. Vcl, Phi, Quartz_QE, and Coal_QE are expressed as fractional values (0–1), whereas permeability (PERM) is given in millidarcies [mD]. The vertical axis represents normalized values*

Table 8
Average values of mineral volumes, reservoir properties, and elastic properties for different rock types and stratigraphic zones

Zone	Rock type	Clay content fraction [v/v]	Porosity [v/v]	Quartz fraction [v/v]	Siderite fraction [v/v]	Coal fraction [v/v]	Young's modulus (static) [GPa]	Poisson's ratio (static) [–]	Permeability horizontal [mD]	Permeability vertical [mD]
Załęże Beds	Coal	0.190	0.093	0.063	0.009	0.645	2.797	0.174	0.186	0.008
	Coal shales	0.400	0.089	0.192	0.011	0.309	3.888	0.141	0.012	
	Mudstones and clays	0.509	0.063	0.347	0.054	0.028	7.231	0.082	0.003	
	Shaly sandstones	0.398	0.058	0.458	0.063	0.022	8.229	0.064	0.007	
	Sandstones	0.221	0.091	0.596	0.052	0.040	12.611	0.052	0.008	
Ruda Beds	Coal	0.182	0.090	0.047	0.005	0.676	2.416	0.177	0.172	0.007
	Coal shales	0.416	0.083	0.160	0.020	0.321	3.799	0.140	0.011	
	Mudstones and clays	0.519	0.056	0.338	0.066	0.021	7.306	0.081	0.003	
	Shaly sandstones	0.396	0.052	0.458	0.081	0.014	8.861	0.059	0.007	
	Sandstones	0.224	0.083	0.600	0.071	0.022	13.412	0.052	0.007	
Saddle Beds	Coal	0.138	0.124	0.059	0.001	0.680	2.277	0.213	0.252	0.007
	Coal shales	0.407	0.089	0.130	0.009	0.366	3.313	0.170	0.012	
	Mudstones and clays	0.562	0.045	0.320	0.056	0.018	7.257	0.096	0.002	
	Shaly sandstones	0.390	0.048	0.480	0.063	0.019	9.124	0.061	0.006	
	Sandstones	0.195	0.078	0.616	0.062	0.050	15.473	0.043	0.006	
Poruba Beds	Coal shales	0.509	0.071	0.101	0.005	0.314	5.549	0.185	0.010	0.003
	Mudstones and clays	0.598	0.022	0.307	0.065	0.009	6.994	0.110	0.002	
	Shaly sandstones	0.415	0.018	0.483	0.075	0.009	7.273	0.080	0.002	
	Sandstones	0.299	0.043	0.577	0.074	0.007	15.877	0.042	0.003	

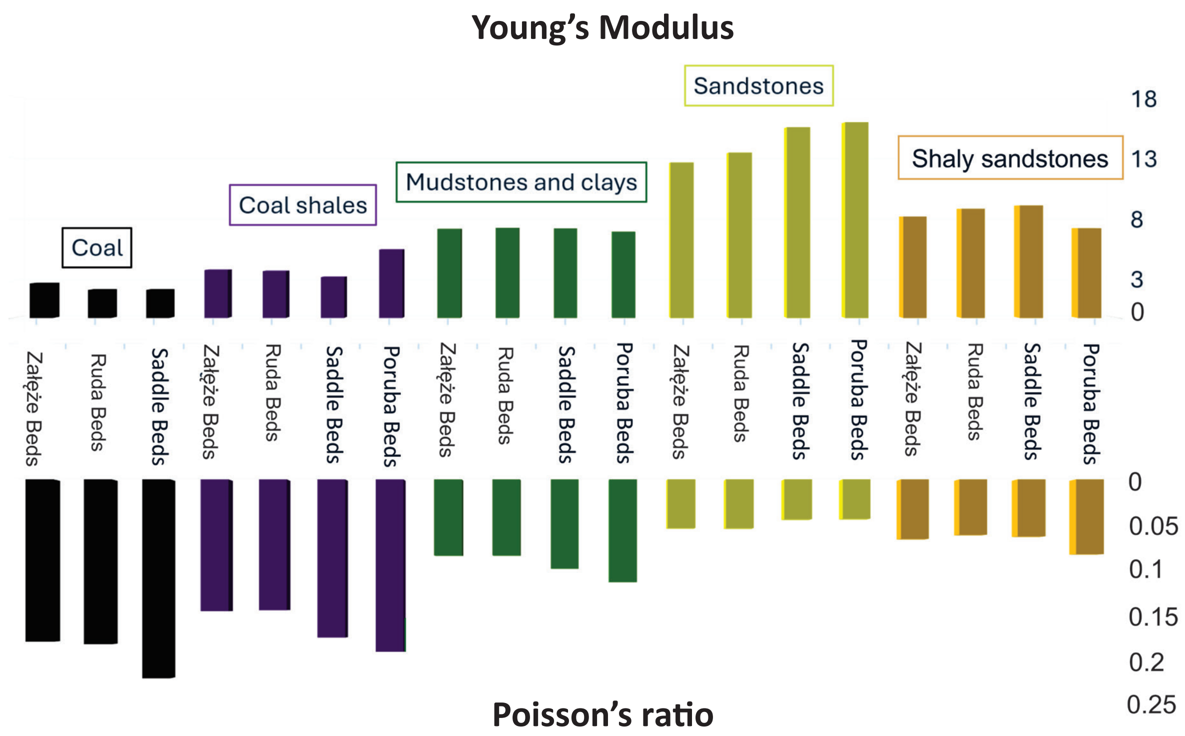

***Fig. 9.** Average values of Young's modulus [GPa] and Poisson's ratio for different rock types within the Załęże Beds, Ruda Beds, Saddle Beds, and Poruba Beds*

CONCLUSIONS

This study presents a comprehensive petrophysical and geomechanical characterization of the Carboniferous coal-bearing formations in the Upper Silesian Coal Basin (USCB). By integrating well log data, core analysis, and petrophysical modeling, robust 1D petrophysical and geomechanical models were developed. The results highlight strong lithological variability and its importance for resource management. The findings emphasize the importance of detailed rock type differentiation when assessing reservoir quality and mechanical behavior. The observed variability in porosity, permeability, and elastic properties across the beds directly affects methane extraction and safe coal exploitation.

Based on the analyses performed, the following conclusions regarding the petrophysical and mechanical characteristics were drawn:

1. Rock type identification: The analyzed productive Carboniferous strata include multi-coal seams from groups 300, 400, 500, and 600, associated with the Załęże, Ruda, Saddle, and Poruba beds, respectively. These seams are interbedded with claystones, mudstones, and sandstones, with their proportions varying depending on the lithostratigraphic bed.
2. Permeability and porosity relationships: Relationships between the laboratory-measured horizontal permeability and porosity were determined. Empirical equations estimating permeability as a function of porosity were developed for each rock type, facilitating permeability predictions.
3. Porosity and permeability variability: Among the analyzed rock types, coal exhibits the highest porosity and permeability values of the rock matrix. In contrast, mudstones and shaly sandstones exhibit anisotropic but very low permeability, whereas sandstones, although isotropic, display very low permeability despite moderate porosity.
4. Permeability in the mining context: Although the rock matrix of the analyzed formations is almost impermeable, it is known that rock

masses in the mining area were subjected to stress relief episodes associated with coal excavations. According to Kędzior (2012), the permeability of the mudstone series, which includes the Orzesze and Załęże beds, can reach values of up to 242 mD, which is comparable to sandstones (Krzanowska 2002).

Regarding the mechanical properties, significant variability in elastic and strength parameters was observed across the rock types:

1. Static and dynamic elastic property relationships: Models defining the relationships between static and dynamic elastic properties were developed, providing a basis for estimating static equivalents of elastic properties in the Upper Silesian Coal Basin.
2. Variability in mechanical properties: Rock types such as coal, shale, mudstone, and sandstone exhibit substantial mechanical variability, which is largely influenced by their internal structure and mineral composition. Coal is characterized by the lowest uniaxial compressive strength (Rc) and Young's modulus (E) due to its high organic content and layered structure, limiting its ability to resist deformation. In contrast, sandstone's granular structure and high quartz content ensure that it exhibits the highest Rc and E values, making it the strongest and stiffest rock type among the analyzed formations.
3. Correlation between Rc, E, and FA: A positive correlation between uniaxial compressive strength (Rc) and Young's modulus (E) was identified, with an especially strong correlation observed between Rc and the friction angle (FA) across various rock types. Sandstones exhibit the highest correlation, attributed to strong intergranular bonding, whereas coal shows a lower correlation due to its cleat structure, which reduces the stress transfer efficiency and shear resistance.
4. Uniaxial compressive to tensile strength ratio (Rc/Ts): The Rc/Ts ratio serves as an important indicator of rock mechanical stability, exhibiting significant variations among rock types. Coal has the highest Rc/Ts ratio, indicating its high susceptibility to cracking under tensile stress due to structural weakness. In contrast, sandstones and mudstones, which have stronger intergranular bonds and lower porosity, exhibit lower and more stable Rc/Ts values, making them more resistant to stress under operational conditions.

Future studies should focus on enhancing the resolution of permeability models through the application of advanced imaging techniques and further investigating the role of fractures in methane migration. These studies are crucial for optimizing resource extraction and ensuring the long-term stability of mining operations in the Upper Silesian Coal Basin. However, it should be noted that the developed petrophysical-geomechanical relationships and regression models are primarily applicable to the geological conditions of the studied area and may not be directly transferable to other settings without further validation.

This research was financially supported by the Ministry of Science and Higher Education (project no. SG-4100-0038/24) and the REM project (Grant Agreement no. 101099061-REM). The funding organizations had no role in study design, data collection, data analysis, interpretation, or manuscript preparation.

REFERENCES

Baran P., Zarębska K., Krzystolik P., Hadro J. & Nunn A., 2014. CO_2-ECBM and CO_2 sequestration in Polish coal seam – Experimental study. *Journal of Sustainable Mining*, 13(2), 22–29. https://doi.org/10.7424/jsm140204.

Bukowska M., 2002. Geomechanical properties of rocks from the rockburst hazard point of view. *Archives of Mining Sciences*, 47(2), 111–138.

Bukowska M., 2003. Własności pokrytyczne skał karbońskich Górnośląskiego Zagłębia Węglowego w warunkach zmiennych prędkości odkształcenia i ciśnień okólnych [Post-critical properties of Carboniferous rocks in the Upper Silesian Coal Basin under varying strain rate and confining pressure conditions]. *Archives of Mining Sciences*, 48(4), 561–575.

Bukowska M., 2006. The probability of rockburst occurrence in the Upper Silesian Coal Basin area dependent on natural mining conditions. *Journal of Mining Science*, 42(6), 570–577. https://doi.org/10.1007/s10913-006-0101-0.

Bukowska M. & Gawryś J., 2010. Właściwości fizyczne węgli GZW w aspekcie wyrzutów gazów i skał [Physical properties of coals in the Upper Silesian Coal Basin in the aspect of coal and methane outbursts]. *Górnictwo i Geoinżynieria*, 34(2), 121–129.

Bukowska M., Sanetra U. & Wadas M., 2012. Chronostratigraphic and depth variability of porosity and strength of hard coals of Upper Silesian Basin. *Gospodarka Surowcami Mineralnymi – Mineral Resources Management*, 28(4), 151–166.

Bukowska M., Sanetra U. & Wadas M., 2016. Zonation of deposits of hard coals of different porosity in the Upper Silesian Coal Basin. *Gospodarka Surowcami Mineralnymi – Mineral Resources Management*, 32(1), 5–24. https://doi.org/10.1515/gospo-2016-0009.

Buła Z., Habryn R., Jachowicz-Zdanowska M. & Żaba J., 2015. The Precambrian and Lower Paleozoic of the Brunovistulicum (eastern part of the Upper Silesian Block, southern Poland) – The state of the art. *Geological Quarterly*, 59(1), 123–134. https://doi.org/10.7306/gq.1203.

Buła Z. & Żaba J., 2008. Struktura prekambryjskiego podłoża wschodniej części bloku górnośląskiego (Brunovistulicum) [Structure of the Precambrian basement of the eastern part of the Upper Silesian block (Brunovistulicum)]. *Przegląd Geologiczny*, 56(6), 473–480.

Castagna J.P., Batzle M.L. & Eastwood R.L., 1985. Relationships between compressional-wave and shear-wave velocities in clastic silicate rocks. *Geophysics*, 50(4), 571–581. https://doi.org/10.1190/1.1441933.

Castagna J.P., Batzle M.L. & Kan T.K., 1993. Rock physics: the link between rock properties and AVO response. [in:] Castagna J.P. & Backus M.M. (eds.), *Offset-Dependent Reflectivity: Theory and Practice of AVO Analysis*, Society of Exploration Geophysicists, 135–171.

Ceglarska-Stefańska G., Stachurski J. & Vogt E., 1995. Porosity of the Polish hard coals. *Archives of Mining Sciences*, 40(3), 303–315.

Chang C., Zoback M.D. & Khaksar A., 2006. Empirical relations between rock strength and physical properties in sedimentary rocks. *Journal of Petroleum Science and Engineering*, 51(3–4), 223–237. https://doi.org/10.1016/j.petrol.2006.01.003b

Chudek M., Duży S., Kleta H., Kłeczek Z., Stoiński K. & Zorychta A., 2000. *Zasady doboru i projektowania obudowy wyrobisk korytarzowych i ich połączeń w zakładach górniczych wydobywających węgiel kamienny*. Wydawnictwo Politechniki Śląskiej, Gliwice.

Dembowski Z., 1972. Ogólne dane o Górnośląskim Zagłębiu Węglowym. [in:] Rühle W. (red.), *Karbon Górnośląskiego Zagłębia Węglowego*, Prace – Instytut Geologiczny, 61, Wydawnictwa Geologiczne, Warszawa, 9–22.

Doveton J.H., 1994. *Geologic Log Analysis Using Computer Methods* (2nd ed.). AAPG Computer Applications in Geology, 2, American Association of Petroleum Geologists, Tulsa.

Drzęźla B., Mendera Z., Barchan A., Głąb L. & Schinohl J., 2000. *Obudowa górnicza: zasady projektowania i doboru obudowy wyrobisk korytarzowych w zakładach górniczych wydobywających węgiel kamienny*. Wydawnictwo Górnicze, Katowice.

Dubiński J., Stec K. & Bukowska M., 2019. Geomechanical and tectonophysical conditions of mining-induced seismicity in the Upper Silesian Coal Basin in Poland: A case study. *Archives of Mining Sciences*, 64(1), 163–180. https://doi.org/10.24425/ams.2019.126278.

Fisher R.A., 1936. The use of multiple measurements in taxonomic problems. *Annals of Eugenics*, 7(2), 179–188. https://doi.org/10.1111/j.1469-1809.1936.tb02137.x.

Fryanov V.N., 2018. Geomechanical substantiation of technology parameters for coal mining in interaction zone of longwall face and gate roadway. *Journal of Mining Science*, 54(6), 906–914. https://doi.org/10.1134/S1062739118065047.

Fu X., Qin Y., Wang G.G.X. & Rudolph R., 2009. Evaluation of coal structure and permeability with the aid of geophysical logging technology. *Fuel*, 88(11), 2278–2285. https://doi.org/10.1016/j.fuel.2009.05.018.

Jura D., 2001. *Morfotektonika i ewolucja różnowiekowej niezgodności w stropie utworów karbonu Górnośląskiego Zagłębia Węglowego*. Prace Naukowe Uniwersytetu Śląskiego w Katowicach, 1952, Wydawnictwo Uniwersytetu Śląskiego, Katowice.

Jureczka J., 1988. Nowe dane o charakterystyce litostratygraficznej kontaktu serii paralicznej i górnośląskiej serii piaskowcowej karbonu zachodniej części GZW. [in:] Lipiarski I. (red.), *XI sympozjum: Geologia formacji węglonośnych Polski: Formacja karbońska, Kraków, 20–22 kwietnia 1988: Materiały*, Wydawnictwo AGH, Kraków, 41–46.

Jureczka J. & Nowak G.J., 2016. Polskie zagłębia węgla kamiennego – przegląd informacji i badań geologicznych. *Przegląd Geologiczny*, 64(9), 617–630.

Kawęcka J., 1988. Struktura porowata węgli kamiennych. [in:] Lasoń M. (red.), *Sorpcja gazów i par a własności polskich węgli kamiennych jako układów dyspersyjnych. Cz. 1*, Zeszyty naukowe Akademii Górniczo-Hutniczej im. Stanisława Staszica, 1212, Chemia, 8, Akademia Górniczo-Hutnicza, Kraków, 69–88.

Kędzior S., 2012. *Przystropowa strefa gazonośna w utworach karbonu południowej części GZW – występowanie, parametry zbiornikowe węgla oraz możliwości pozyskania metanu*. Wydawnictwo Uniwersytetu Śląskiego, Katowice.

Kotas A., 1982. Zarys budowy geologicznej Górnośląskiego Zagłębia Węglowego. [in:] Różkowski A. & Ślósarz J. (red.), *Przewodnik LIV Zjazdu Polskiego Towarzystwa Geologicznego, Sosnowiec, 23–25 września 1982*, Wydawnictwa Geologiczne, Warszawa, 45–72.

Kotas A. & Malczyk W., 1972. Seria paraliczna piętra namuru dolnego Górnośląskiego Zagłębia Węglowego. [in:] Rühle W. (red.), *Karbon Górnośląskiego Zagłębia Węglowego*, Prace – Instytut Geologiczny, 61, Wydawnictwa Geologiczne, Warszawa, 329–411.

Krzanowska A., 2002. *Dodatek nr 1 do dokumentacji geologicznej złoża węgla kamiennego Pawłowice w kat. C1, C2*. CAG Państwowy Instytut Geologiczny [unpublished].

Li D., Wang E., Kong X., Ali M. & Wang D., 2019. Mechanical behaviors and acoustic emission fractal characteristics of coal specimens with a pre-existing flaw of various inclinations under uniaxial compression. *International Journal of Rock Mechanics and Mining Sciences*, 116, 38–51. https://doi.org/10.1016/j.ijrmms.2019.03.022.

Majkrzak M., 2019. Wpływ zmian wybranych parametrów pokładu węgla kamiennego na przebieg i efektywność procesu eksploatacji metanu. *Nafta-Gaz*, 75(5), 254–264. https://doi.org/10.18668/NG.2019.05.03.

Małkowski P. & Niedbalski Z., 2024. The meaning of average compressive and tensile strength for Hoek–Brown mi constant determination. *Archives of Mining Sciences*, 69(3), 485–508. https://doi.org/10.24425/ams.2024.151447.

Murariu G., Dinca L. & Munteanu D., 2025. Trends and applications of principal component analysis in forestry research: A literature and bibliometric review. *Forests*, 16(7), 1155. https://doi.org/10.3390/f16071155.

Moska R. & Kędzior S., 2015. Możliwości występowania niekonwencjonalnych akumulacji gazu ziemnego w serii mułowcowej na terenie GZW. *Nafta-Gaz*, 71(10), 729–736.

Pearson K., 1901. On lines and planes of closest fit to systems of points in space. *The London, Edinburgh, and Dublin Philosophical Magazine and Journal of Science*, 2(11), 559–572. https://doi.org/10.1080/14786440109462720.

Probierz K., Marcisz M. & Sobolewski A., 2012. Rozpoznanie warunków geologicznych występowania węgla koksowego w rejonie Jastrzębia dla potrzeb projektu „Inteligentna koksownia" [The recognition of geological conditions of coking coal occurrence in the Jastrzębie area for the project: Smart coke plant fulfilling requirements of best available techniques]. *Biuletyn Państwowego Instytutu Geologicznego*, 452, 245–256.

Prusek S., Krause E. & Skiba J., 2020. Designing coal panels in the conditions of associated methane and spontaneous fire hazards. *International Journal of Mining Science and Technology*, 30(4), 525–531. https://doi.org/10.1016/j.ijmst.2020.05.015.

Ranjith P.G. & Perera M.S.A., 2012. Effects of cleat performance on strength reduction of coal in CO_2 sequestration. *Energy*, 45(1), 1069–1075. https://doi.org/10.1016/j.energy.2012.05.041.

Rybacki E., Reinicke A., Meier T., Makasi M. & Dresen G., 2015. What controls the mechanical properties of shale rocks? – Part I: Strength and Young's modulus. *Journal of Petroleum Science and Engineering*, 135, 702–722. https://doi.org/10.1016/j.petrol.2015.10.028.

Singh B., Jethwa J.L. & Dube A.K., 1995. A classification system for support pressure in tunnels and caverns. *Journal of Rock Mechanics and Tunnelling Technology*, 1, 13–24.

Słoczyński T., Drozd A. & Sowiżdżał K., 2017. Ocena potencjału zasobowego CBM (coal bed methane) oraz możliwości występowania akumulacji gazu ziemnego typu tight w formacjach piaskowcowo-mułowcowych GZW. *Nafta-Gaz*, 73(10), 711–722. https://doi.org/10.18668/NG.2017.10.03.

Sobczyk E.J. 2022. *Uciążliwość eksploatacji złóż węgla kamiennego wynikająca z warunków geologicznych i górniczych* [Onerousness of hard coal mining resulting from geological and mining conditions]. Wydawnictwo Instytutu Gospodarki Surowcami Mineralnymi i Energią PAN, Kraków.

Song J., Liu Y., Luo Y., Yang F. & Hu D., 2024. Effect of lateral confining pressure on shale's mechanical properties and its implications for fracture conductivity. *Applied Sciences*, 14(13), 5825. https://doi.org/10.3390/app14135825.

Srinaiah J., Raju D., Udayalaxmi G. & Ramadass G., 2017. Application of well logging techniques for identification of coal seams: A case study of Auranga Coalfield, Latehar District, Jharkhand State, India. *Journal of Geology & Geophysics*, 7(1), 322. https://doi.org/10.4172/2381-8719.1000322.

Strugała A., 2001. Porowatość węgli bitumicznych. *Gospodarka Surowcami Mineralnymi – Mineral Resources Management*, 17(2), 5–17.

Wood D.A. & Cai J., 2022. Coal-bed methane reservoir characterization using well-log data. [in:] Wood D.A. & Cai J. (eds.), *Sustainable Geoscience for Natural Gas Subsurface Systems*, The Fundamentals and Sustainable Advances in Natural Gas Science and Engineering, 2, Gulf Professional Publishing, 243–274. https://doi.org/10.1016/B978-0-323-85465-8.00006-6.

Wood G.H., Kehn T.M., Carter M.D. & Culbertson W.C., 1983. *Coal Resource Classification System of the U.S. Geological Survey*. U.S. Geological Survey Circular, 891, U.S. Geological Survey, Denver, Co. https://doi.org/10.3133/cir891.

Wójcicki A. & Jureczka J., 2010. *Rozpoznanie formacji i struktur do bezpiecznego geologicznego składowania CO_2 wraz z ich programem monitorowania. Raport merytoryczny nr 3: Segment I, rejon GZW*. https://skladowanie.pgi.gov.pl/twiki/pub/CO2/WynikiPrac/I-0-wst%EAp.pdf [access: 12.05.2026].

Xie H., Zhang L., Sun X., Wang X. & Cao Y., 2023. Tensile failure characteristics of coal and its 3D cohesive zone model. *Geotechnical and Geological Engineering*, 41(4), 2299–2312. https://doi.org/10.1007/s10706-023-02398-5.

Ye Y., 2025. A comprehensive review of principal component analysis. *Academic Journal of Science and Technology*, 17(1), 224–227. https://doi.org/10.54097/5 mmrkr11.

Zarębska K. & Ceglarska-Stefańska G., 2006. The kinetics of sorption of CO_2 and CH_4 mixtures with regard to possibility of CO_2 sequestration in the coal seams. *Gospodarka Surowcami Mineralnymi – Mineral Resources Management*, 22(3), 301–309.